Mapping of wave packet dynamics at conical intersections by time- and frequency-resolved fluorescence spectroscopy : a computational study

Chen, Lipeng; Gelin, Maxim F.; Zhao, Yang; Domcke, Wolfgang

2019

Chen, L., Gelin, M. F., Zhao, Y. & Domcke, W. (2019). Mapping of wave packet dynamics at conical intersections by time- and frequency-resolved fluorescence spectroscopy : a computational study. Journal of Physical Chemistry Letters, 10(19), 5873-5880. https://dx.doi.org/10.1021/acs.jpclett.9b02208

https://hdl.handle.net/10356/150601

https://doi.org/10.1021/acs.jpclett.9b02208

Mapping of Wave-Packet Dynamics at Conical Intersections by Time- and Frequency-Resolved Fluorescence Spectroscopy: A Computational Study

Lipeng Chen,*,† Maxim F. Gelin,† Yang Zhao,‡ and Wolfgang Domcke†

†*Department of Chemistry, Technische Universität München, D-85747, Garching,Germany*

‡*Division of Materials Science, Nanyang Technological University, 50 Nanyang Avenue, Singapore 639798*

E-mail: chen0846@gmail.com

Abstract

Monitoring of wave-packet dynamics at conical intersections by time- and frequency-resolved fluorescence spectroscopy has been investigated theoretically for a three-state two-mode model of a conical intersection coupled to a dissipative environment. The ideal and the actually measurable time- and frequency-gated fluorescence spectra were accurately and efficiently simulated by combining the hierarchy equations-of-motion method for dissipative quantum dynamics with the methodology of the equation-of-motion phase-matching approach for the calculation of spectroscopic signals. It is shown that time- and frequency-resolved fluorescence spectra reveal essential aspects of the wave-packet dynamics at conical intersections and the effects of environment-induced dissipation. The results of the present work indicate that fluorescence up-conversion spectroscopy with femtosecond time resolution is an efficient tool for the characterization of ultrafast dynamics at conical intersections.

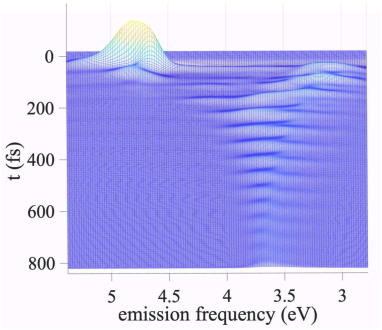

Conical intersections (CIs) of adiabatic electronic potential energy surfaces (PESs) are generic features in polyatomic molecules exhibiting points (in general, multi-dimensional seams) of exact degeneracy of electronic PESs in nuclear coordinate space.[1,2] CIs play a significant role in large variety of photophysical and photochemical processes: they lead to a complete breakdown of the Born-Oppenheimer (BO) approximation and result in the strongly mixed quantum dynamics of electrons and nuclei. It is nowadays generally accepted that CIs provide the microscopic mechanism of ultrafast (femtosecond) electronic relaxation in polyatomic systems.[3–5]

As non-adiabatic nuclear dynamics near CIs can lead to extremely short lifetimes of excited electronic states, it is difficult to directly probe and characterize the effect of CIs in photochemical reactions. With the availability of ultrafast UV/vis/IR lasers, the explicit detection of electron-vibrational dynamics at CIs has increasingly become feasible. Radiationless electronic transitions caused by CIs were studied by pump-probe photoelectron spectroscopy[6–8] as well as by transient absorption pump-probe and pump-dump-probe spectroscopy.[9–11] Transient-grating spectroscopy identified the key vibrational modes which drive the CI-mediated isomerization of retinal on a sub-50 fs timescale.[12] In recent years, two-dimensional (2D) spectroscopy has emerged as a powerful technique in vis/IR.[13] The extension of 2D spectroscopy to the UV spectral range has opened new possibilities in the studies of ultrafast dynamics at CIs.[14–16] 2D electron-vibrational (2DEV) spectroscopy has also been recently applied to probe CIs.[17] The development of ultrafast X-ray sources with

femtosecond/attosecond pulse durations provides novel tools for scrutinizing CIs. It has been demonstrated that time-resolved X-ray spectra are sensitive to the electronic and structural evolution of chromophores with CIs.[18,19] A hybrid technique implementing UV/vis femtosecond pump pulse and a pair of attosecond X-ray pulses was theoretically proposed for probing electronic coherence created by the CI.[20] Femtosecond electron diffraction has also emerged as a powerful tool for the characterization of nuclear wave packets at CIs in real time and with atomistic spacial resolution.[21]

However, extraction of information about non-adiabatic dynamics at CIs from time-resolved signals is not straightforward. Suppose we wish to probe a CI of the PES of two excited electronic states in a polyatomic molecule. In the widely used transient-absorption pump-probe spectroscopy, the wave-packet motion at a CI of excited electronic states is projected onto the electronic ground state of the molecule (stimulated emission) as well as onto certain higher-lying electronic states (excited-state absorption). The detected signal is the sum of stimulated emission, excited-state absorption and ground-state bleach (the latter does not contain information on excited-state dynamics). In femtosecond time-resolved photoelectron spectroscopy, the wave-packet motion at a CI of excited electronic states is projected onto the continuum of states of the ionized molecule and the ejected photoelectron. The fluorescence up-conversion signal[22–24] can be viewed as the projection of the wave-packet motion at the CI onto the electronic ground state. In this sense, the fluorescence signal has the simplest interpretation and is most amenable to a theoretical simulation. In this Letter, we establish a direct connection between the excited-state wave-packet dynamics and time- and frequency-resolved spontaneous emission (SE) spectra for a model of a CI and demonstrate that this connection provides a detailed characterization of the ultrafast internal conversion processes triggered by the CI.

Several groups employed the numerically efficient and accurate hierarchy equation of motion (HEOM) method to simulate electron-vibrational dynamics at CIs.[25–30] In particular, we previously used the HEOM method to analyze electronic population dynamics and

vibrational wave-packet evolutions of a two-state two-mode CI (which represents the Condon-active part of the chromophore) which is weakly-to-moderately coupled to a dissipative bath (which represents all remaining vibrational modes of the chromophore as well as the vibrational degrees of freedom of the solvent).[25] In the present work, we perform accurate simulations of time- and frequency-resolved SE spectra for the model of Ref.[25] The system consists of three electronic states (the electronic ground state $|0\rangle$ and two excited states $|1\rangle$, $|2\rangle$ forming the CI) which are strongly coupled to two vibrational modes:

$$H^{(S)} = \sum_{k=0,1,2} |k\rangle(h_k + \epsilon_k)\langle k| + (|1\rangle\langle 2| + |2\rangle\langle 1|)\lambda Q_c. \tag{1}$$

Here ϵ_k is the energy of the kth electronic state ($\epsilon_0 = 0$) and

$$h_k = \frac{1}{2}\sum_{j=c,t} \hbar\Omega_j\{P_j^2 + Q_j^2\} + \kappa_k Q_t \tag{2}$$

are the vibrational Hamiltonians in which Q_j, P_j and Ω_j are the dimensionless coordinate, dimensionless momentum and frequency of the coupling ($j = c$) and tuning ($j = t$) modes, κ_k are the electron-vibrational coupling constants ($\kappa_0 \equiv 0$) while the parameter λ controls the nonadiabatic coupling strength at the CI. We assume that each system vibrational mode is bilinearly coupled to a harmonic bath (see Ref.[25] for a more detailed discussion). The bath Hamiltonian is written as

$$H^{(B)} = \{|0\rangle\langle 0| + |1\rangle\langle 1| + |2\rangle\langle 2|\}\sum_{j=c,t}\sum_{\alpha}\frac{1}{2}\hbar\omega_{\alpha,j}\{p_{\alpha,j}^2 + q_{\alpha,j}^2\} \tag{3}$$

where $p_{\alpha,j}$, $q_{\alpha,j}$ and $\omega_{\alpha,j}$ are the dimensionless momentum, coordinate, and frequency of αth bath mode coupled to the tuning ($j = t$) and coupling ($j = c$) mode of the system. The system-bath interaction Hamiltonian assumes the form

$$H^{(SB)} = \{|1\rangle\langle 1| + |2\rangle\langle 2|\}\sum_{j=c,t}\sum_{\alpha}\{c_{\alpha,j}q_{\alpha,j}Q_j\} \tag{4}$$

where the $c_{\alpha,j}$ are the system-bath coupling constants. The effect of the bath on the system dynamics is fully characterized by the spectral density $J_j(\omega) = \sum_\alpha c_{\alpha,j}^2 \delta(\omega - \omega_{\alpha,j})$ ($j = c,\, t$). We adopt the Drude spectral density $J_j(\omega) = 2\Lambda_j \Gamma_j \omega/(\omega^2 + \Gamma_j^2)$. Here Λ_j are the vibrational damping strengths (or, equivalently, the bath-induced reorganization energies) while Γ_j^{-1} are the bath relaxation times for the tuning ($j = t$) and coupling ($j = c$) modes.

The HEOM method allows the numerically exact computation of the time evolution of the reduced density matrix $\rho(t)$ of the system in terms of the coupled operator equations[31,32]

$$\partial_t \boldsymbol{\rho}(t) = -\frac{i}{\hbar}\left[H^{(S)}, \boldsymbol{\rho}(t)\right] - \boldsymbol{\mathcal{R}}\boldsymbol{\rho}(t) \tag{5}$$

where $\boldsymbol{\rho}$ denotes a set of density operators $\{\rho_{l_c,l_t}\}$ of which $\rho_{00}(t) \equiv \rho(t)$ and all other ρ_{l_c,l_t} are auxiliary density operators. The explicit form of the dissipation operator $\boldsymbol{\mathcal{R}}$ for the present model can be found in Ref.[25]

In a fluorescence up-conversion experiment, the system interacts with pump (α = p for pump) and gate (α = f for fluorescence) laser pulses.[33] The corresponding interaction Hamiltonians in the rotating wave approximation (RWA) are written as

$$H_\alpha(t) = -\eta_\alpha E_\alpha(t - t_\alpha)\{e^{i\omega_\alpha t} X + e^{-i\omega_\alpha t} X^\dagger\}, \tag{6}$$

where η_α, ω_α, t_α and $E_\alpha(t)$ denote the system-field coupling parameter, the carrier frequency, the arrival time, and the dimensionless envelope of the αth pulse, while the raising and lowering components of the transition dipole moment operator are defined as

$$X = |0\rangle\langle 2|, \quad X^\dagger = |2\rangle\langle 0| \tag{7}$$

(state $|2\rangle$ is assumed to be optically bright, while state $|1\rangle$ is optically dark). We calculate the time- and frequency-resolved SE spectra $S(t, \omega_{\rm f})$ by employing the two-pulse variant of the equation-of-motion phase-matching approach (EOM-PMA).[34,35] The basic equations are

summarized as follows:

$$
\begin{aligned}
S(t,\omega_{\rm f}) &= {\rm Im}\{A(t,\omega_{\rm f})\},\\
A(t,\omega_{\rm f}) &= {\rm Tr}\left\{e^{-i\omega_{\rm f}t}X^{\dagger}\left[\bar{\rho}_{00}(t)-\rho_{00}(t)\right]\right\}+O(\eta_{\rm f}^{3}),\\
\partial_t\boldsymbol{\rho}(t) &= -\frac{i}{\hbar}\left[H^{(S)}-H_{\rm p}(t),\boldsymbol{\rho}(t)\right]-(\boldsymbol{\mathcal{R}}+\mathcal{D})\boldsymbol{\rho}(t),\\
\partial_t\bar{\boldsymbol{\rho}}(t) &= -\frac{i}{\hbar}\left[H^{(S)}-H_{\rm p}(t),\bar{\boldsymbol{\rho}}(t)\right]+\frac{i}{\hbar}e^{i\omega_{\rm f}t}X\bar{\boldsymbol{\rho}}(t)-(\boldsymbol{\mathcal{R}}+\mathcal{D})\bar{\boldsymbol{\rho}}(t).
\end{aligned}
\tag{8}
$$

Here $\boldsymbol{\rho}(t)$ and $\bar{\boldsymbol{\rho}}(t)$ are the two sets of auxiliary density matrices involved in the HEOM calculation, $\rho_{00}(t)$ and $\bar{\rho}_{00}(t)$ are the corresponding reduced system density matrices, and optical dephasing is described by the operator $\mathcal{D}\rho(t)=\xi|0\rangle\langle 0|\rho(t)(1-|0\rangle\langle 0|)+{\rm H.c.}$ in which ξ is the dephasing rate.

$S(t,\omega_{\rm f})$ yields the so-called ideal SE spectrum, which is defined as the rate of emission of photons of frequency $\omega_{\rm f}$ at time t. The simultaneous precise detection of $\omega_{\rm f}$ and t violates the Heisenberg uncertainty relation. The actually measurable time- and frequency-gated (TFG) SE spectrum is obtained by the convolution of $S(t,\omega_{\rm f})$ with the TFG function Φ[34,35]

$$
S_{\rm TFG}(t,\omega_{\rm f})\sim {\rm Im}\int_{-\infty}^{\infty}d\omega^{'}\int_{-\infty}^{\infty}dt^{'}\Phi(t-t',\omega_{\rm f}-\omega^{'})A(t',\omega^{'})
\tag{9}
$$

where

$$
\Phi(\tau,\Omega)=E_{\rm f}(-\tau)\int_{-\infty}^{-\tau}d\vartheta E_{\rm f}(\vartheta)\exp\left\{(\gamma+i\Omega)(\tau+\vartheta)\right\}.
\tag{10}
$$

Here the parameter $0\leq\gamma<\infty$ controls the spectral resolution ($\gamma=0$ corresponds to ideal frequency resolution), while duration of the gate pulse controls the time resolution ($E_{\rm f}(t)\rightarrow\delta(t)$ corresponds to ideal temporal resolution). Eq. (10) shows that $\Phi(\tau,\Omega)$ cannot be approximated as $\delta(\tau)\delta(\Omega)$ (see Refs.[33–37] for detailed discussions of the interconnection of ideal and TFG SE signals).

For the numerical simulations, we adopt parameters of the system Hamiltonian $H^{(S)}$ which mimic the $S_2(\pi\pi^*)-S_1(n\pi^*)$ CI in pyrazine.[25,38] More precisely, S_1, S_2 designate the

adiabatic electronic states and PES (which are ordered by energy) and $n\pi^*, \pi\pi^*$ designate the diabatic electronic states which preserve their electronic character. The vibrational frequencies of the tuning and coupling modes are $\hbar\Omega_t = 0.074$ eV ($2\pi/\Omega_t = 56$ fs) and $\hbar\Omega_c = 0.118$ eV ($2\pi/\Omega_c = 35$ fs). The intrastate coupling constants are $\kappa_1 = -0.105$ eV and $\kappa_2 = 0.149$ eV. The interstate coupling strength is $\lambda = 0.262$ eV. The vertical excitation energies are $\epsilon_1 = 3.94$ eV and $\epsilon_2 = 4.84$ eV. The cuts of the resulting adiabatic PESs are shown in Fig. 1. The system-field coupling is fixed at $\eta_\mathrm{p} = 0.01$ eV, ensuring weak system-field interaction ($S(t,\omega_\mathrm{f}) \sim \eta_\mathrm{p}^2$). The pump pulse is of Gaussian shape and assumed to be in electronic resonance with the S_2 state ($\hbar\omega_\mathrm{p} = \epsilon_2$) and short on the system dynamics timescale ($E_\mathrm{p}(t) = \exp\{-[(t-t_p)/\tau_\mathrm{p}]^2\}$, $\tau_\mathrm{p} = 5$ fs and $t_p = 8\tau_\mathrm{p}$). The gate pulse is also taken as Gaussian ($E_\mathrm{f}(t) = \exp\{-(t/\tau_\mathrm{f})^2\}$) and provides good temporal ($\tau_\mathrm{f} = 10$ fs) and spectral ($\gamma = 0$) resolution. Optical dephasing is moderate ($\xi = 0.01$ eV, $\xi^{-1} = 66$ fs), the bath relaxation time is fixed at $\Gamma_t^{-1} = \Gamma_c^{-1} = 50$ fs, while the system-bath couplings $\Lambda_j (j = c, t)$ are varied. The ideal signals (8) are evaluated by a numerical solution of the driven HEOMs for $\boldsymbol{\rho}(t)$ and $\bar{\boldsymbol{\rho}}(t)$ as described in Ref.[25]

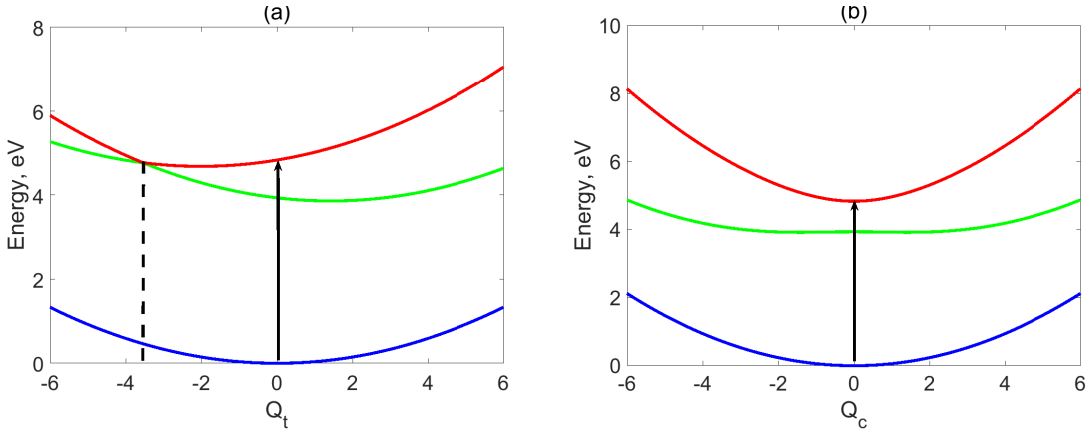

Figure 1: Cuts through the adiabatic PESs of the electronic ground state (blue), S_1 state (green) and S_2 state (red) of the pyrazine model along the normal coordinates Q_t for $Q_c = 0$ (a) and along Q_c for $Q_t = 0$ (b). Vertical excitation by a short pump pulse is indicated by the arrow. Position of the CI at $Q_t \approx 3.5$, $Q_c = 0$ is marked by the dashed line in (a).

The present model of the CI possesses a single Condon-active vibrational mode, the tuning mode Q_t, and the wave-packet dynamics along this mode is expected to reveal itself in

the time- and frequency-resolved SE. The coupling mode Q_c, on the other hand, does not drive coherent wave-packet dynamics, as can be expected from the anharmonic, but undisplaced, PESs in Fig. 1(b). We thus begin with a brief analysis of the adiabatic probability density $P_{\mathrm{S}_2}(Q_t, t)$ of the tuning mode projected on the upper adiabatic state (S_2), which is expressed through the S_2-projected reduced density matrix in the coordinate representation, $\langle \mathrm{S}_2|\rho(Q_t, Q_t', Q_c, Q_c', t)|\mathrm{S}_2\rangle$, by integrating out the coupling mode:[38]

$$P_{\mathrm{S}_2}(Q_t, t) = \int_{-\infty}^{\infty} \langle \mathrm{S}_2|\rho(Q_t, Q_t, Q_c, Q_c, t)|\mathrm{S}_2\rangle dQ_c.$$

$P_{\mathrm{S}_2}(Q_t, t)$ is computed by assuming an instantaneous (at $t = 0$) promotion of the ground-state vibrational wave function of the electronic ground state to the bright $\pi\pi^*$ state (see Fig. 1). It represents the probability density to find the system in the adiabatic electronic state S_2 and at the nuclear position Q_t at time t. The reduced density matrix is calculated in the diabatic electronic representation and then transformed to the adiabatic representation.[25] Fig. 2 shows $P_{\mathrm{S}_2}(Q_t, t)$ for different system-bath couplings $\Lambda_c = \Lambda_t = 0$ (a), 2 cm^{-1} (b) 10 cm^{-1} (c) and 60 cm^{-1} (d). These values of Λ_j cover the range of potentially relevant vibrational relaxation times, from infinity (a) to about 1 ps (d), which is a typical cooling time of vibrationally hot solutes in liquid environments. Irrespective of the system-bath coupling strength, the wave packet exhibits short-time ($t < 100$ fs) underdamped motion. The wave-packet density moves towards negative Q_t following the gradient of the S_2 surface (see Fig. 1). Within half of a vibrational period of the tuning mode (~ 28 fs), the wave packet reaches the CI and partially transfers to the adiabatic S_1 surface, where it experiences a gradient in the opposite direction. This results in coherent short-time wave-packet dynamics within the range $-6 \lesssim Q_t \lesssim 6$, according to the initial energy contained in the wave packet. In contrast to the short-time dynamics, the time evolution of $P_{\mathrm{S}_2}(Q_t, t)$ for $t > 200$ fs depends significantly on the system-bath coupling. For the isolated CI, the structure of $P_{\mathrm{S}_2}(Q_t, t)$ becomes increasingly irregular with time (panel (a)). For weak coupling to the bath, the

$S_2 \rightarrow S_1$ radiationless transition is still incomplete at $t \sim 1$ ps. However, the irregular structures are suppressed and $P_{S_2}(Q_t, t)$ reveals oscillatory ridges around $Q_t \approx -2$ and 4 (panel (b)). A stronger coupling to the environment (panel (c)) produces a smoothened version of $P_{S_2}(Q_t, t)$, which shows regular oscillatory structures with a period $2\pi/\Omega_t = 56$ fs. If the system-bath coupling increases further, $P_{S_2}(Q_t, t)$ exhibits qualitatively different behavior (panel (d)). The bath facilitates irreversible $S_2 \rightarrow S_1$ population transfer on a ~ 1 ps timescale and the probability density $P_{S_2}(Q_t, t)$ gradually contracts, becoming concentrated around $Q_t \approx 1.6$ which corresponds to the minimum of the S_1 state (see Fig. 1).

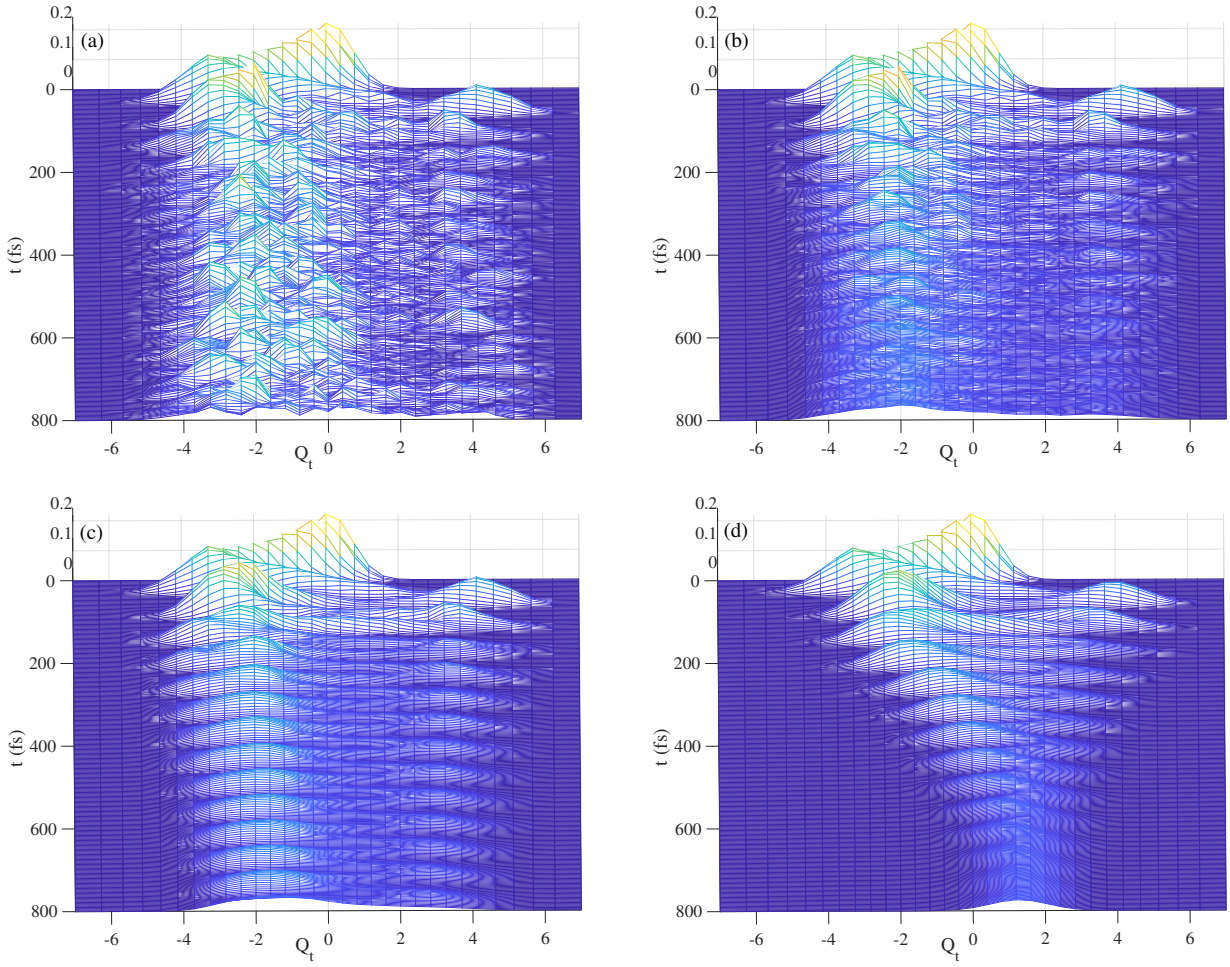

Figure 2: Time dependent probability density $P_{S_2}(Q_t, t)$ of the tuning mode in the upper adiabatic PES S_2 for different system bath coupling strengths $\Lambda_t = \Lambda_t = 0$ (a), 2 cm^{-1} (b), 10 cm^{-1} (c) and 60 cm^{-1} (d).

Let us now consider SE signals. Fig. 3 shows computed ideal SE spectra which correspond to perfect time and frequency resolution and thus contain the maximum of information on the wave-packet dynamics. Panels (a) through (d) correspond to the system-bath coupling strengths $\Lambda_t = \Lambda_c = 0$, 2 cm^{-1}, 10 cm^{-1}, and 60 cm^{-1}, as in Fig. 2. For the isolated CI (panel (a)), $S(t, \omega_\mathrm{f})$ exhibits two well-separated emission bands arising from the S_2 state (left) and the S_1 state (right), respectively. Emission from the S_1 state occurs through $S_2 \rightarrow S_1$ internal conversion at very short time scales ($t < 50$ fs) due to intensity borrowing induced by the nonadiabatic coupling. The S_2 emission is overall more intense than the S_1 emission for weak system-bath coupling (panels (a) and (b)). For stronger system-bath coupling (panels (c) and (d)), on the other hand, the emission from the S_2 state dies away at longer times due to radiationless depopulation of the S_2 state.

The S_2 and S_1 states can be viewed as coherent emission sources, and the superposition of emissions from different vibronic levels of the S_2 and S_1 states produce pronounced and broad interference patterns covering the spectral domain from 3 to 5 eV (panel (a)). A very weak system-bath coupling largely suppresses and smoothens erratic features in the time- and frequency-resolved spectra, showing that the wave-packet dynamics at CIs is highly sensitive to external perturbations (panel (b)), which is characteristic for chaotic dynamics. With a larger but still weak system-bath coupling, $S(t, \omega_\mathrm{f})$ reveals almost complete $S_2 \rightarrow S_1$ population transfer on a timescale of ~ 500 fs (panel (c)). For a moderate system-bath coupling (panel (d)), emission from the S_2 state disappears after about hundred femtoseconds, while the fast $S_2 \rightarrow S_1$ population transfer produces a broad (~ 1 eV) initial emission from S_1 state. The spectral width of this emission narrows with time, being centered around 3.7 eV at 800 fs. This manifests the dissipation of excess vibrational energy (available after the $S_2 \rightarrow S_1$ radiationless transition) to the bath, which drives the system to the energy minimum of the S_1 state. This is the mechanism behind the famous rule of Kasha.

While ideal time- and frequency-resolved SE spectra provide perfect time and frequency resolution, TFG SE spectra are limited by the fundamental time-frequency uncertainty prin-

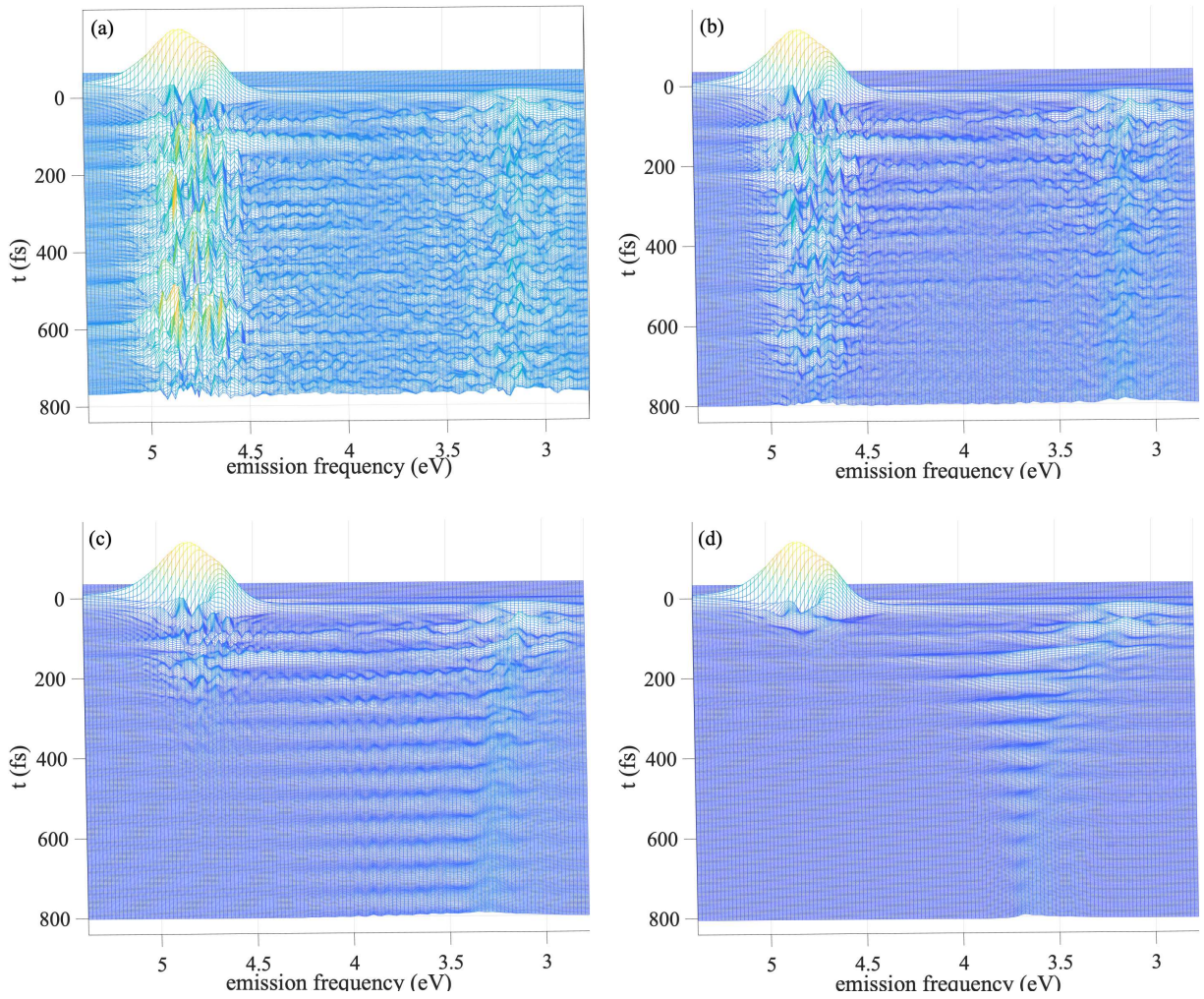

Figure 3: Ideal time- and frequency-resolved SE spectra $S(t, \omega_{\mathrm{f}})$ for different system-bath couplings: $\Lambda_t = \Lambda_c = 0$ (a), 2 cm^{-1} (b), 10 cm^{-1} (c) and 60 cm^{-1} (d).

ciple. The TFG SE spectra calculated from the ideal spectra presented in Fig. 3 are plotted in Fig. 4, assuming good temporal resolution ($\tau_\mathrm{f} = 10$ fs) and perfect frequency resolution ($\gamma = 0$). The erratic features dominating the ideal spectrum in Fig. 3(a) are wiped out in the TFG spectrum of Fig. 4(a) due to finite resolution in time. The TFG SE signal is smooth and clearly reveals vibrational wave-packet dynamics in the S_2 and S_1 states. With a slight increase of the system-bath coupling (panel (b)), $S_\mathrm{TFG}(t, \omega_\mathrm{f})$ starts to exhibit additional quenching of the S_2 population at longer emission times due to $S_2 \rightarrow S_1$ internal conversion. The TFG SE spectra in panels (c) and (d) resemble the corresponding ideal SE spectra in Fig. 3(c) and (d), reflecting the wave-packet motion of the tuning mode in the S_2 and S_1 states. With longer gate pulses (e.g., $\tau_\mathrm{f} = 50$ fs or 100 fs), vibrational motion can no longer be captured, while emissions from individual vibronic levels of the S_2 and S_1 states can be detected, as shown in Figs. S5, S6 in the Supporting Information.

In the present simplified model for pyrazine, the S_1 state borrows roughly 20 % of the intensity of the S_2 state in the stationary absorption spectrum, which agrees qualitatively with the experimental observations.[39] In the absence of dissipation, the fluorescence intensities roughly reflect this intensity ratio (Fig. 4(a)) and the fluorescence from S_1 should therefore be easy to detect. In the presence of dissipation, on the other hand, the fluorescence from S_2 is rapidly quenched, while the fluorescence from S_1 survives (Fig. 4(d)). At first glance, the comparison of Figs. 4(a) and (d) seems to indicate that fluorescence photons are lost by the inclusion of dissipation. This is, however, not the case (in the absence of competing relaxation processes). The fluorescence is just emitted at later times and therefore is not visible in Fig. 4.

The S_2-projected probability densities $P_{S_2}(Q_t, t)$ in Fig. 2 and the spectroscopic signals in Figs. 3 and 4 were computed for the same values of the model parameters. These figures reveal remarkable similarity, proving that the ideal signal $S(t, \omega_\mathrm{f})$ and the measurable signal $S_\mathrm{TFG}(t, \omega_\mathrm{f})$ deliver projections of the wave packet in the S_2 state. Some difference between $P_{S_2}(Q_t, t)$ and $S(t, \omega_\mathrm{f})$, $S_\mathrm{TFG}(t, \omega_\mathrm{f})$ can be seen around $t \sim t_p$ because the Raman

and fluorescence contributions to the SE spectra coexist for overlapping pump and gate pulses.

The similarity between $P_{S_2}(Q_t, t)$ and $S(t, \omega_f)$ can be made almost quantitative. If the pump pulse duration τ_p and the optical dephasing time ξ^{-1} are short on the system dynamics time scale, one can show under certain plausible assumptions that $S(t, \omega_f)$ and $P_{S_2}(Q_t, t)$ approximately coincide if $\omega_f \approx \kappa_2 Q_t$.[35] The comparison of Figs. 2 and 3 reveals that this correspondence works quite well. For example, the initial width of the distribution $P_{S_2}(Q_t, t)$ ($-6 < Q_t < 6$) corresponds to a width of ~ 1.8 eV in the frequency domain, which correlates with the width of ~ 2 eV of $S(t, \omega_f)$. The widths of the two ridges of $P_{S_2}(Q_t, t)$ ($-4 < Q_t < 0$ and $0 < Q_t < 4$ in Figs. 2(b)) become ridges of a width 0.6 eV in Fig. 3(b). On the other hand, the probability densities of the coupling mode $P_{S_2}(Q_c, t)$, which are presented in Figs. S1 - S4 in the Supporting Information, are not mapped out by the SE signals. In this respect, the TFG spectrum does not reveal the complete information on the nonadiabatic dynamics at the CI.

To summarize, we have systematically studied the monitoring of the excited-state wavepacket dynamics by fluorescence up-conversion spectroscopy for a three-state two-mode model mimicking the $S_2 - S_1$ CI of pyrazine immersed in a dissipative environment. We combined the HEOM method for the simulation of dissipative quantum dynamics with the EOM-PMA methodology for the calculation of spectroscopic signals. With these methods, accurate simulations of dissipative nonadiabatic dynamics and systematic comparisons of vibrational wavepackets, ideal time- and frequency-resolved SE spectra and TFG SE spectra at CIs have become possible. We found that TFG SE spectra provide information on the wave-packet dynamics of tuning modes of CIs and are very sensitive to bath-induced dissipation.

It is possible to extend the present work towards the simulation of TFG SE spectra of more realistic and complete (24 dimensional) models of pyrazine, which include quadratic and higher-order vibrational and vibronic couplings, the dynamics of which involves a cascade

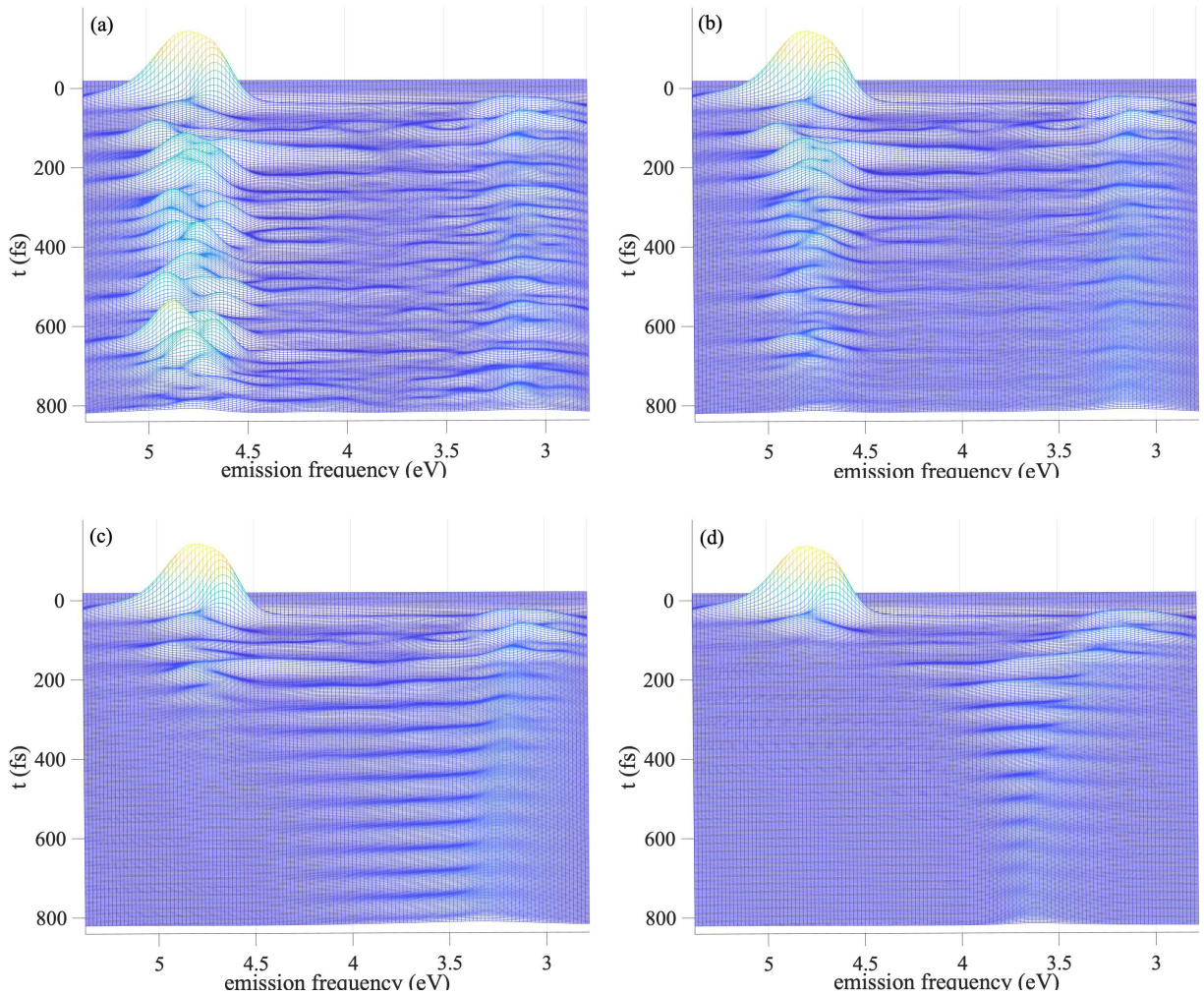

Figure 4: TFG SE spectra $S_{\mathrm{TFG}}(t, \omega_S)$ in the case of a good time resolution ($\tau_{\mathrm{f}} = 10$ fs), a perfect spectral resolution ($\gamma = 0$) and different system-bath couplings: $\Lambda_t = \Lambda_c = 0$ (a), 2 cm^{-1} (b), 10 cm^{-1} (c) and 60 cm^{-1} (d).

of transitions through CIs.[40,41] This can be achieved, for example, by the combination of the numerically efficient multiple Davydov Ansatz method with a general framework for the evaluation of the third-order nonlinear response functions.[42,43] It is also of great interest to implement methods for *ab initio* on-the-fly calculations of TFG SE spectra for polyatomic molecules by using, e.g., the semiclassical thawed Gaussian method,[44] the multiple spawning method,[45] or the multiconfigurational Ehrenfest method.[46] Work in these directions is in progress.

The TFG SE spectrum can be viewed as a projection of the wave-packet motion at the CI onto the electronic ground state. The results of the present work demonstrate that the TFG SE signal mimics the time evolution of this wave packet in fine details, provided at least one of the excited states has a non-vanishing transition dipole moment with the electronic ground state. Since sub-50 fs temporal resolution in fluorescence up-conversion already has been demonstrated[47], TFG SE spectroscopy potentially can become a powerful and widely applicable tool for the characterization of wave-packet dynamics of CIs in the Franck-Condon region of polyatomic molecules.

Acknowledgement

L. P. C. acknowledges support by a postdoctoral fellowship of the Alexander von Humboldt-Foundation. M. F. G. and W. D. acknowledge support from the Deutsche Forschungsgemeinschaft through a research grant and through the DFG Cluster of Excellence Munich-Centre for Advanced Photonics (http://www.munich-photonics.de).

Supporting Information

1. Time-dependent probability densities of the tuning and coupling modes for different system-bath couplings (Figs. S1-S4)

2. TFG SE spectra detected with poor time resolution (Figs. S5, S6).

References

(1) Robb, M. A.; Bernardi, F.; Olivucci, M. Conical Intersections as a Mechanistic Feature of Organic Photochemistry. *Pure Appl. Chem.* **1995**, *67*, 783-789.

(2) Yarkony, D. R. Diabolical Conical Intersections. *Rev. Mod. Phys.* **1996**, *68*, 985-1013.

(3) Domcke, W.; Yarkony, D. R.; Köppel, H. *Conical Intersections: Electronic Structure, Dynamics and Spectroscopy*; World Scientific: Singapore; 2004.

(4) Worth, G. A.; Cederbaum, L. S. Beyond Born-Oppenheimer: Molecular Dynamics Through a Conical Intersection. *Annu. Rev. Phys. Chem.* **2004**, *55*, 127-158.

(5) Domcke, W.; Yarkony, D. R. Role of Conical Intersections in Molecular Spectroscopy and Photoinduced Chemical Dynamics. *Annu. Rev. Phys. Chem.* **2012**, *63*, 325-352.

(6) Stolow, A.; Bragg, A. E.; Neumark, D. M. Femtosecond Time-Resolved Photoelectron Spectroscopy. *Chem. Rev.* **2004**, *104*, 1719-1758.

(7) Horio, T.; Spesyvtsev, R.; Nagashima, K.; Ingle, R. A.; Suzuki, Y.; Suzuki, T. Full Observation of Ultrafast Cascaded Radiationless Transitions from $S2(\pi\pi^*)$ State of Pyrazine Using Vacuum Ultraviolet Photoelectron Imaging. *J. Chem. Phys.* **2016**, *145*, 044306-044315.

(8) Horio, T.; Suzuki, Y.; Suzuki, T. Ultrafast Photodynamics of Pyrazine in the Vacuum Ultraviolet Region Studied by Time-Resolved Photoelectron Imaging Using 7.8-eV Pulses. *J. Chem. Phys.* **2016**, *145*, 044307-044314.

(9) Polli, D.; Altoè, P.; Weingart, O.; Spillane, K. M.; Manzoni, C.; Brida, D.; Tomasello, G.; Orlandi, G.; Kukura, P.; Mathies, R. A.; Garavelli, M.; Cerullo, G. Conical Intersection Dynamics of the Primary Photoisomerization Event in Vision. *Nature.* **2010**, *467*, 440-442.

(10) Wei, Z.; Nakamura, T.; Takeuchi, S.; Tahara, T. Tracking of the Nuclear Wavepacket Motion in Cyanine Photoisomerization by Ultrafast Pump-Dump-Probe Spectroscopy. *J. Am. Chem. Soc.* **2011**, *133*, 8205-8210.

(11) Liebel, M.; Schnedermann, C.; Kukura, P. Vibrationally Coherent Crossing and Coupling of Electronic States during Internal Conversion in β-Carotene. *Phys. Rev. Lett.* **2014**, *112*, 198302-198306.

(12) Johnson, P. J. M.; Halpin, A.; Morizumi, T.; Prokhorenko, V. I.; Ernst, O. P.; Miller, R. J. D. Local Vibrational Coherences Drive the Primary Photochemistry of Vision. *Nat. Chem.* **2015**, *7*, 980-986.

(13) Fuller, F. D.; Ogilvie, J. P. Experimental Implementations of Two-Dimensional Fourier Transform Electronic Spectroscopy. *Annu. Rev. Phys. Chem.* **2015**, *66*, 667-690.

(14) Auböck, G.; Consani, C.; van Mourik, F.; Chergui, M. Ultrabroadband Femtosecond Two-Dimensional Ultraviolet Transient Absorption. *Opt. Lett.* **2012**, *37*, 2337-2339.

(15) West, B. A.; Moran, A. M. Two-Dimensional Electronic Spectroscopy in the Ultraviolet Wavelength Range. *J. Phys. Chem. Lett.* **2012**, *3*, 2575-2581.

(16) Kitney-Hayes, K. A.; Ferro, A. A.; Tiwari, V.; Jonas, D. M. Two-dimensional Fourier Transform Electronic Spectroscopy at a Conical Intersection. *J. Chem. Phys.* **2014**, *140*, 124312-124330.

(17) Wu, E. C.; Ge, Q; Arsenault, E. A.; Lewis, N. H. C.; Gruenke, N. L.; Head-Gordon, M. J.; Fleming, G. R. Two-Dimensional Electronic-Vibrational Spectroscopic Study of Conical Intersection Dynamics: an Experimental and Electronic Structure Study. *Phys. Chem. Chem. Phys.* **2019**, *21*, 14153-14163.

(18) Chergui, M.; Collet, E. Photoinduced Structural Dynamics of Molecular Systems Mapped by Time-Resolved X-Ray Methods. *Chem. Rev.* **2017**, *117*, 11025-11065.

(19) Kowalewski, M.; Fingerhut, B. P.; Dorfman, K. E.; Bennett, K.; Mukamel, S. Simulating Coherent Multidimensional Spectroscopy of Nonadiabatic Molecular Processes: From the Infrared to the X-Ray Regime. *Chem. Rev.* **2017**, *117*, 12165-12226.

(20) Kowalewski, M.; Bennett, K.; Dorfman, K. E.; Mukamel, S. Catching Conical Intersections in the Act: Monitoring Transient Electronic Coherences by Attosecond Stimulated X-Ray Raman Signals. *Phys. Rev. Lett.* **2015**, *115*, 193003-193008.

(21) Ischenko, A. A.; Weber, P. M.; Miller, R. J. D. Capturing Chemistry in Action with Electrons: Realization of Atomically Resolved Reaction Dynamics. *Chem. Rev.* **2017**, *117*, 11066-11124.

(22) Shah, J. Ultrafast Luminescence Spectroscopy Using Sum Frequency Generation. *IEEE J. Quant. Electron.* **1988**, *24*, 276-288.

(23) Sarkar, N.; Takeuchi, S.; Tahara, T. Vibronic Relaxation of Polyatomic Molecules in Nonpolar Solvent: Femtosecond Anisotropy/Intensity Measurements of the Sn and S1 Fluorescence of Tetracene. *J. Phys. Chem A.* **1999**, *103*, 4808-4814.

(24) Braem, O.; Penfold, T. J.; Cannizzo, A.; Chergui, M. A Femtosecond Fluorescence Study of Vibrational Relaxation and Cooling Dynamics of UV Dyes. *Phys. Chem. Chem. Phys.* **2012**, *14*, 3513-3519.

(25) Chen, L. P.; Gelin, M. F.; Chernyak, V. Y.; Domcke, W.; Zhao, Y. Dissipative Dynamics at Conical Intersections: Simulations with the Hierarchy Equations of Motion Method. *Faraday Discuss.* **2016**, *194*, 61-80.

(26) Dijkstra, A. G.; Prokhorenko, V. I. Simulation of Photo-Excited Adenine in Water with a Hierarchy of Equations of Motion Approach. *J. Chem. Phys.* **2017**, *147*, 064102-064109.

(27) Ikeda, T.; Tanimura, Y. Phase-Space Wavepacket Dynamics of Internal Conversion via

Conical Intersection: Multi-State Quantum Fokker-Planck Equation Approach. *Chem. Phys.* **2018**, *515*, 203-213.

(28) Duan, H. G.; Miller, R.J. D.; Thorwart, M. Impact of Vibrational Coherence on the Quantum Yield at a Conical Intersection. *J. Phys. Chem. Lett.* **2016**, *7*, 3491-3496.

(29) Qi, D. L.; Duan, H. G.; Sun, Z. R.; Miller, R.J. D.; Thorwart, M. Tracking an Electronic Wave Packet in the Vicinity of a Conical Intersection. *J. Chem. Phys.* **2017**, *147*, 074101-074107.

(30) Duan, H. G.; Qi, D. L.; Sun, Z. R.; Miller, R.J. D.; Thorwart, M. Signature of the Geometric Phase in the Wave Packet Dynamics on Hypersurfaces. *Chem. Phys.* **2018**, *515*, 21-27.

(31) Ishizaki, A.; Tanimura, Y. Quantum Dynamics of a System Strongly Coupled to a Low Temperature Colored Noise Bath: Reduced Hierarchy Equations Approach. *J. Phys. Soc. Jpn.* **2005**, *74*, 3131-3134.

(32) Tanimura, Y. Stochastic Liouville, Langevin, Fokker-Planck, and Master Equation Approaches to Quantum Dissipative Systems. *J. Phys. Soc. Jpn.* **2006**, *75*, 082001-082039.

(33) Eberly, J.H.; Wodkiewicz, K. The Time-Dependent Physical Spectrum of Light. *J. Opt. Soc. Am.* **1977**, *67*, 1252-1261.

(34) Gelin, M. F.; Egorova, D.; Domcke, W. A New Method for the Calculation of Two-Pulse Time- and Frequency-Resolved Spectra. *Chem. Phys.* **2005**, *312*, 135-143.

(35) Egorova, D.; Gelin, M. F.; Domcke, W. Time- and Frequency-Resolved Fluorescence Spectra of Nonadiabatic Dissipative Systems: What Photons Can Tell Us. *J. Chem. Phys.* **2005**, *122*, 134504-134518.

(36) Mukamel, S.; Ciordas-Ciurdariu, C.; Khidekel, V. Time-Frequency and Coordinate-Momentum Wigner Wavepackets in Nonlinear Spectroscopy. *Adv. Chem. Phys.* **1997**, *101*, 345-372.

(37) Mukamel, S. Wigner Spectrogram Representations of Hetrodyne-Detected Four-Wave-Mixing and Fluorescence Up-Conversion. *J. Chem. Phys.* **1997**, *107*, 4165-4171.

(38) Schneider, R.; Domcke, W.; Köppel, H. Aspects of Dissipative Electronic and Vibrational Dynamics of Strongly Vibronically Coupled Systems. *J. Chem. Phys.* **1990**, *92*, 1045-1061.

(39) Yamazaki, I.; Murao, T.; Yamanaka, T.; Yoshihara, K. Intramolecular Electronic Relaxation and Photoisomerization Processes in the Isolated Azabenzene Molecules Pyridine, Pyrazine and Pyrimidine. *Faraday Discuss. Chem. Soc.* **1983**, *75*, 395-405.

(40) Raab, A.; Worth, G. A.; Meyer, H. D.; Cederbaum, L. S. Molecular Dynamics of Pyrazine after Excitation to the S_2 Electronic State Using a Realistic 24-mode Model Hamiltonian. *J. Chem. Phys.* **1999**, *110*, 936-946.

(41) Sala, M.; Guérin, S.; Gatti, F. Quantum Dynamics of the Photostability of Pyrazine. *Phys. Chem. Chem. Phys.* **2015**, *17*, 29518-29530.

(42) Chen, L. P.; Gelin, M. F.; Domcke, W. Multimode Quantum Dynamics with Multiple Davydov D_2 Trial States: Application to a 24-dimensional Conical Intersection Model. *J. Chem. Phys.* **2019**, *150*, 024101-024113.

(43) Sun, K. W.; Gelin, M. F.; Chernyak, V. Y.; Zhao, Y. Davydov Ansatz as Efficient Tool for the Simulation of Nonlinear Optical Response of Molecular Aggregates. *J. Chem. Phys.* **2015**, *142*, 212448-212457.

(44) Begušić, T.; Roulet, J. Vaníček, J. On-the-fly Ab Initio Semiclassical Evaluation of Time-Resolved Electronic Spectra. *J. Chem. Phys.* **2018**, *149*, 244115-244129.

(45) Curchod, B. F. E.; Martinez, T. J. Ab Initio Nonadiabatic Quantum Molecular Dynamics. *Chem. Rev.* **2018**, *118*, 3305-3336.

(46) Makhov, D. V.; Symonds, C.; Fernandez-Alberti, S.; Shalashilin, D. V. Ab Initio Quantum Direct Dynamics Simulations of Ultrafast Photochemistry with Multiconfigurational Ehrenfest Approach. *Chem. Phys.* **2017**, *493*, 200-218.

(47) Kumpulainen,T.; Lang, B.; Rosspeintner, A.; Vauthey, E. Ultrafast Elementary Photochemical Processes of Organic Molecules in Liquid Solution. *Chem. Rev.* **2017**, *117*, 10826-10939.